Article

Investigating Surface Settlements During Shield Tunneling Using Numerical Analysis

Ruixia He [1,2], Ziwen Zhou [2,3],*, Shuai Li [1],* and Sai Vanapalli [2]

1 Department of Civil and Transportation Engineering, Henan University of Urban Construction, Pingdingshan 467036, China; 30010501@huuc.edu.cn
2 Department of Civil Engineering, University of Ottawa, Ottawa, ON K1N 6N5, Canada
3 Nanjing Institute of Environmental Sciences, Ministry of Ecology and Environment of the People's Republic of China, Nanjing 210042, China; sai.vanapalli@uottawa.ca
* Correspondence: zhouziwenhhu@163.com (Z.Z.); li-82.28@163.com (S.L.)

Abstract: The development of the subway system in Shenyang City, China, plays a vital role in alleviating traffic congestion and promoting sustainable societal growth. However, the deformation of the surface caused by the tunneling of the shield presents a significant threat to the structural integrity of Shenyang Subway Line 2 and adjacent geotechnical structures. To tackle this challenge, a set of FEA (finite element analysis) simulations were carried out to examine surface deformation under various construction scenarios for Line 2. These simulations were compared with empirical formulas and numerical analyses conducted using Midas GTS NX 2019 software, in addition to actual site measurements. The outcomes of the finite element analysis (FEA) demonstrated a closer alignment with the empirical data than with traditional formulas. The maximum deformation was observed to be approximately twice as large as the equivalent diameter at the back of the excavation face. The analysis indicated that surface deformation is inversely correlated with overburden thickness (H), soil elasticity (E), and the grout filling rate of the shield tail (ψ), while it is directly proportional to the shield's outer diameter (D). This study provides important methods used in the shield tunneling process employed in the Shenyang subway and suggests that the developed methodologies may be applicable to similar subway projects.

Keywords: shield tunnel; surface settlement; numerical simulation; empirical method; overburden thickness; geotechnical properties

1. Introduction

The rapid expansion of transit networks in China has played a vital role in promoting the sustainability of tunnel infrastructure development over the past two decades [1]. As a result, predicting and managing surface settlement due to shield tunneling construction (STC) has emerged as a central theme of extensive research [2–4]. Single-circular shield tunneling machines are commonly employed to excavate and line tunnels in soft and other unstable geological conditions [5].

Shield tunneling encompasses the construction process, eliminating the need for temporary shoring. During Earth Pressure Balance (EPB) operations, shield mechanisms are deployed to control surface deformations and mitigate potential damage to adjacent infrastructure [6–10]. To achieve these crucial construction and design objectives, a precise estimation of the magnitude and distribution of settlements in both horizontal and vertical planes is imperative. Surface settlement is generally determined through three

distinct methods: experimental testing, empirical and theoretical models, and numerical modeling [11].

Experimental testing serves as a reliable method for investigating surface settlement resulting from shield tunneling [12–15]. The empirical data collected from field tests, using various techniques across a range of soil types, significantly inform the development of construction and design protocols for shield tunneling [16]. Research has utilized transparent soil models to simulate and observe surface settlement during shield tunneling construction, with the findings indicating a decrease in settlement magnitude as the tunnel depth increases [17]. Furthermore, laboratory tests conducted under 1 g conditions have been performed to examine surface settlement in unsaturated sandy soil [6]. These experimental methodologies enhance our understanding of settlement behavior and contribute to the refinement of shield tunneling practices.

A number of empirical formulae, theoretical models, and simplified representations have been proposed for the evaluation of the ground displacements caused by the shield tunneling method [18,19]. Gui et al. (2013) employed an empirical formula to estimate the settlement pattern above a tunnel, followed a Gaussian distribution, and utilized FEA to predict excessive settlements that could potentially damage adjacent structures [20]. Fang et al. (2017) studied surface deformation resulting from shield tunneling [6]. Researchers have developed analytical techniques to compute the surface settlement induced by tunneling [21,22]. Zhu et al. (2017a, 2017b) provided a comprehensive review of methodologies for estimating and calculating surface settlement, together with definitions of parameters like volume loss, peak surface settlement, as well as the width of the settlement trough [23,24]. These studies have shown that the profile of the settlement trough conforms to the Gaussian curve. Although analytical methods offer advantages in addressing ground surface settlement, they face significant limitations in practical applications. For instance, they rely on numerous assumptions and simplifications inherent to analytical methods, including the assumptions of soil isotropy, plane strain conditions, and modulus of elasticity. Such assumptions may prove invalid when actual site conditions are reduced to a 2D (two-dimensional) scenario with plane strain. Furthermore, some assumptions disregard the influence of the tunnel face and adjacent ground, resulting in questionable settlement estimates [25–27]. Notably, Brinkgreve's (2005) research indicates that the Mohr–Coulomb model has limited capacity for accurately representing soil deformation prior to failure [28].

Numerous investigations have demonstrated that numerical modeling methodologies can accurately simulate surface settlement induced by tunneling operations [29–31]. A 3D (three-dimensional) finite difference model (FDM) was used to compute the Double-O-Tube shield tunneling process [24,32,33]. Gao et al. (2014) developed a 3D non-linear FEM for the Z1 subway line in Tianjin, China [34]. Mathew et al. (2013) assessed the efficacy of 2D and 3D finite element analysis (FEA) in predicting ground displacement [35]. To examine the impact of tail void grouting, 3D finite element simulations were performed on a simplified scenario involving a tunnel excavated through homogeneous sandy soil beneath the groundwater table [36]. Several factors, such as construction techniques, surface pavement, traffic disturbances, significant surface settlement, and inaccuracies in manual measurements, can lead to discrepancies between field-monitoring data and analytical results [37]. Furthermore, long-term field observations often include consolidation settlements that are typically not considered in numerical models, potentially resulting in field-measured settlements exceeding numerical predictions [38].

Shenyang Subway Line 2 constitutes a critical element of Shenyang's metropolitan transit network, extending 31.88 km and comprising 26 subterranean stations. The excavation of Line 2 was carried out using a single-diameter Earth Pressure Balance (EPB) shield machine. During the construction period, the shield machine navigated through regions

prone to settlement, implementing rigorous control measures to minimize ground displacement. The project's complexity was exacerbated by the site's intricate geological features, presenting substantial challenges. It is essential to predict the extent of the excavation-induced damage zone and potential dynamic hazards, including surface movement, to ensure the safety of the entire excavation process before initiating operations [39,40].

This study is structured with the following objectives: (1) to develop a three-dimensional (3D) numerical model for predicting surface settlement; (2) to simulate surface settlement across various construction scenarios, considering tunnel parameters such as overburden thickness and other geotechnical properties; and (3) to validate the model's efficacy and reliability by integrating empirical formulas and field measurement data. The methodologies presented in this paper provide valuable technical insights for the shield tunnel construction of the Shenyang metro Line 2 and can be adapted for use in other similar metro tunneling projects.

2. Research Methods

2.1. Numerical Modeling

2.1.1. FEM Methodology

Midas GTS (Geotechnical Analysis and Design Software) is a powerful tool for analyzing soil–structure interactions and simulating a wide range of scenarios frequently encountered in geotechnical engineering. The software utilizes a comprehensive set of modeling equations and constitutive relationships to accurately characterize the response of soil and rock masses under varying loading states. The following section outlines key concepts associated with the modeling equations and constitutive relationships implemented in Midas GTS.

The constitutive models used in Midas GTS are all based on the laws of elasticity and plasticity. The linear elastic models adhere to Hooke's law, which gives a linear correlation between stress and strain, as defined by Young's modulus (E) and a constant Poisson's ratio (ν). In comparison, non-linear elastic models use more complicated relationships to describe the non-linear stress–strain response of the materials under specific circumstances. In the area of plasticity models, Midas GTS contains the Mohr–Coulomb and Drucker–Prager (DP) models. The first one is widely used to determine the yield surface of materials like soil and rock, which is characterized by the cohesion (c) and the angle of internal friction (φ), and it enables the simulation of plastic deformation and soil failure. The second one expands the Mohr–Coulomb model to describe material response under three-dimensional stresses, making it particularly suited to cohesive materials.

Midas GTS employs the FEM to solve the governing equations of geotechnical problems. By discretizing the soil region in finite elements, the software facilitates the analysis of stress, strain, and displacement within the soil structure. This discretion permits a precise evaluation of how soil and rock respond under various simulated conditions, offering a thorough understanding of their behavior.

2.1.2. Model Establishment

The foundational soil within the study area is composed of three distinct layers, clayey soil, sandy soil, and gravelly sandy soil, which belong to the Quaternary formation and are arranged from the tunnel's crown to its base, as determined by geological surveys. Numerical models offer enhanced accuracy in predicting surface settlements by accounting for the shield tail void, grout filling, and soil disturbance around the tunnel. A 3D FEM model has been constructed for the Shengyang Subway Line 2, as depicted in Figure 1a. The model dimensions are 54 m along the x-axis, 36 m along the y-axis, and 32 m along the z-axis. The tunnel progresses along the y-axis, with the model's upper boundary set

at the natural ground level and the lower boundary 12 m beneath the tunnel floor. The computational domain is discretized into 32,086 four-node quadrilateral elements.
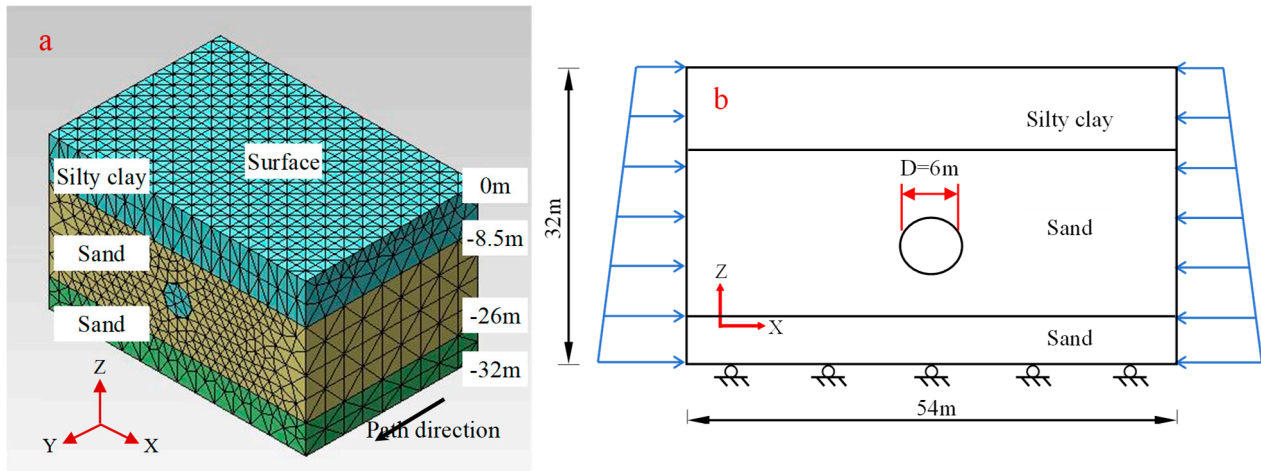
Figure 1. (**a**) Finite element model; (**b**) loads in excavation step.

The modeling process is predicated on several assumptions: (1) the earth's surface and all soil layers are considered to have a uniform and horizontal stratification; (2) the soil's behaviors are presumed to adhere to the Mohr-Coulomb failure criterion and to exhibit an elastic–plastic stressstrain behavior; and (3) groundwater flow is disregarded, and soil deformation is assumed to be time-independent.

Regarding the boundary conditions, the model is subjected to rest compression in the *x*-direction (left and right sides) and *y*-direction (front and back sides), and it is fully constrained at the bottom, with the top surface remaining unobstructed. It is anticipated that the ground pressure at rest will gradually change with depth. The simulation was performed under drained conditions. It is estimated that the earth pressure in soil chamber *P* is roughly equal to the sum of the supporting pressure and the soil's static water pressure. This is expressed by the following formula:

$$P = K \cdot P_0, \tag{1}$$

where P_0 is the total of the static water pressure and the supporting pressure. The value of *K* could typically be assumed to be 1.0 in clayey soil [41]. Figure 1b displays a typical finite element mesh used in the investigation. The mesh dimensions for the excavated portion are established at 0.8 m, while the grid dimensions for the unexcavated area are set at 1 m. The tunnel, with a diameter of 6 m, is constructed within a sandy soil stratum. It is unavoidable that the surrounding soil will be impacted by the tunnel structure's excavation.

2.1.3. Parameters Setup of Soils and Structures

Three representative sections (K18 + 288.163, K18 + 192.163, and K18 + 048.163) were selected for modeling calculations to enhance the credibility and general applicability of the numerical model. Tables 1–3 provide specifics on the mechanical and physical characteristics of the tunnel lining, equivalent layer, and soil for each section, respectively. The simulation of a 24 m tunnel excavation was conducted using a step-by-step approach, comprising 20 sequential stages, each with an excavation length of 1.2 m.

Table 1. Soil properties and other parameters of each layer of soil and structures at section K18 + 288.163.

Soil and Structure	Thickness (m)	Poisson Ratio	Density (kN/m^3)	Young's Modulus (GPa)	Cohesion (kPa)	Friction Angle (°)
Silty clay	8.5	0.29	19.0	5.200	30.0	
Sand1	17.5	0.26	19.5	30.000	0.0	35.0
Sand2	6.0	0.25	19.9	36.000	3.9	37.8
Lining	-	0.20	26.0	20.400	-	-
Softening slurry	-	0.30	21.0	0.001	-	-
Hardening slurry	-	0.25	21.0	0.050	-	-

Table 2. Soil properties and other parameters of each layer of soil and structures at section K18 + 192.163.

Soil and Structure	Thickness (m)	Poisson Ratio	Density (kN/m^3)	Young's Modulus (GPa)	Cohesion (kPa)	Friction Angle (°)
Fine sand	1	0.27	18.5	7.300	6.0	20.0
Sand1	15	0.26	19.5	30.000	0.0	35.0
Sand2	6	0.25	19.9	36.000	3.9	37.8
Lining	-	0.20	26.0	20.400	-	-
Softening slurry	-	0.30	21.0	0.001	-	-
Hardening slurry	-	0.25	21.0	0.050	-	-

Table 3. Soil properties and other parameters of each layer of soil and structures at section K18 + 048.163.

Soil and Structure	Thickness (m)	Poisson Ratio	Density (kN/m^3)	Young's Modulus (GPa)	Cohesion (kPa)	Friction Angle (°)
Silty clay	8	0.29	19.0	5.200	30	18
Sand	12	0.26	19.5	30.000	0	35
Medium coarse sand	10	0.26	19.5	15.000	0	30
Lining	-	0.20	26.0	20.400	-	-
Softening slurry	-	0.30	21.0	0.001	-	-
Hardening slurry	-	0.25	21.0	0.050	-	-

2.2. Empirical Method

Over the past few decades, various empirical and semi-empirical methods have been devised to address the challenges in geotechnical engineering. Prominent among these are the Peck method [42,43], the Oteo method [44,45], and the Romo–Diaz method [46,47]. Notably, the most widely used empirical formulation in practice is the one created by Peck [43]. According to this formulation, a Gaussian distribution curve can accurately represent the ground surface settlement profile (see Figure 2). The mathematical representation of this model is as follows:

$$S(x) = S_{\max}(x) \exp\left(-\frac{x^2}{2i^2}\right), \tag{2}$$

where i is the trough width parameter, which is the distance between the tunnel center and the inflection point, m; S_x is the ground surface settlement at a distance x from the tunnel center, m; and $S_{\max}$ is the maximum ground surface settlement at the vertical tunnel axis, m.
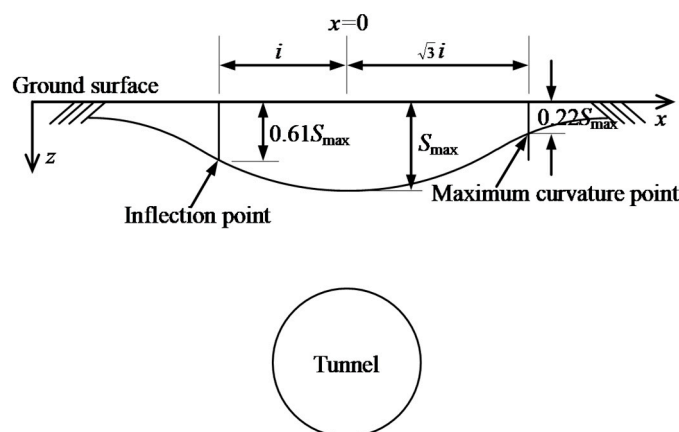
Figure 2. Transverse settlement trough.

In actuality, the phrase "volume loss" (V_s), which is a percentage of the hypothetical excavated volume of the tunnel, m³, is frequently used to describe the settlements brought on by tunneling. The relationship between S_{max} and V_s could be expressed as follows by integrating Equation (2):

$$S_{max} = \frac{V_s}{\sqrt{2\pi}i}, \tag{3}$$

$$V_s = V_l \pi (D/2)^2, \tag{4}$$

where D is the outside tunnel diameter, m, and V_l is the ground volume loss rate, m³/d. Therefore, the only factors influencing the surface settlement curve's magnitude and shape for a given D are the volume loss V_s and the trough width parameter i.

A number of formulas have been put out to estimate the trough width parameter, i. The most widely used expression, summarized as Equation (5), is used in this study, which was proposed by Knothe [48]. The parameter i is related to the friction angle of the soil (φ) and tunnel depth (Z_0) in the form of $i = f(\varphi, Z_0)$. The trough width parameter i for the soils with three typical tunnel sections are listed in Table 4, derived from Equation (5).

$$i = \frac{Z_0}{\sqrt{2\pi} \tan(45° - \frac{\varphi}{2})}. \tag{5}$$

Table 4. Trough width parameter i of different sections and layers.

| Cross Section	Soil and Structure	Thickness (m)	Friction Angle (°)	Trough Width Parameter i
K18 + 288.163	Silty clay	8.5	18.0	4.67
	Sand 1	17.5	35.0	13.41
	Sand 2	6.0	37.8	4.89
K18 + 192.163	Fine sand	1.0	20.0	0.57
	Sand 1	15.0	350	11.50
	Sand 2	6.0	37.8	4.89
K18 + 048.163	Silty clay	8.0	18.0	4.39
	Sand	12.0	35.0	9.20
	Medium coarse sand	10.0	30.0	6.91

3. Results

Many factors affect surface settlement during shield tunneling, including the overburden thickness (H), shield outer diameter (D), the relative burial depth (H/D), soil properties,

and construction details. Establishing an accurate correlation between these factors and surface settlement is challenging due to the limited availability of empirical and experimental data. However, the FEM provides a robust framework for handling complex boundary conditions and delivering reliable results [49]. This study employs FEM to simulate and quantify surface settlement across various construction scenarios, as well as to investigate the interplay between different parameters and the resulting ground settlement during tunneling. Numerical simulations were performed on three specific sections (K18 + 288.163, K18 + 192.163, and K18 + 048.163), demonstrating consistent patterns among them. Notably, the section K18 + 288.163 is highlighted as a representative case in subsequent analyses.

3.1. Surface Settlements with Different Steps

The simulation of a 24 m tunnel excavation was conducted using a sequential method, comprising 20 stages, each excavating 1.2 m. As depicted in Figure 3, the surface settlement at K18 + 288.163 escalates to a significant value of 10.15 mm upon the shield machine reaching the 20th stage. Upon examination of the symmetry in the measured settlement trough curve, it is observed to be roughly symmetrical about the tunnel's central axis.
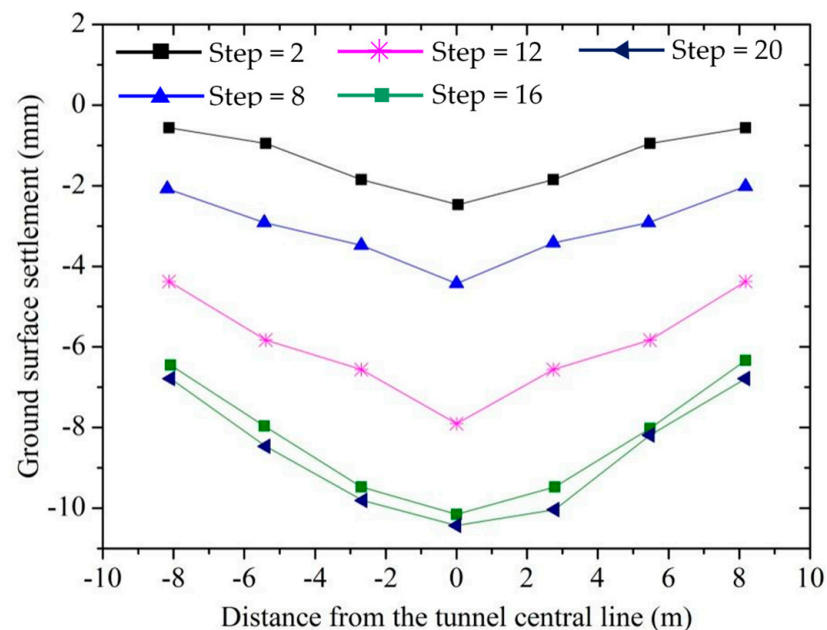
Figure 3. The surface settlement trough section K18 + 288.163 for different excavation steps.

Important surface stations along the tunnel axis were chosen as observation sites in order to look into the longitudinal trend of settlement. Settlement patterns at varying distances from the tunnel entrance were independently modeled using Midas GTS. Figure 4 delineates the 20 stages of excavation, providing a detailed depiction of the tunneling process. It is observed that prior to the shield's arrival, the soil experiences a minor uplift of 1–2 mm, attributable to the extrusion effect at the tunnel face. But as the barrier moves forward, the soil starts to settle, and the settlement becomes more intense. When the shield tail reaches the twentieth excavation stage, the peak settlement is noted.
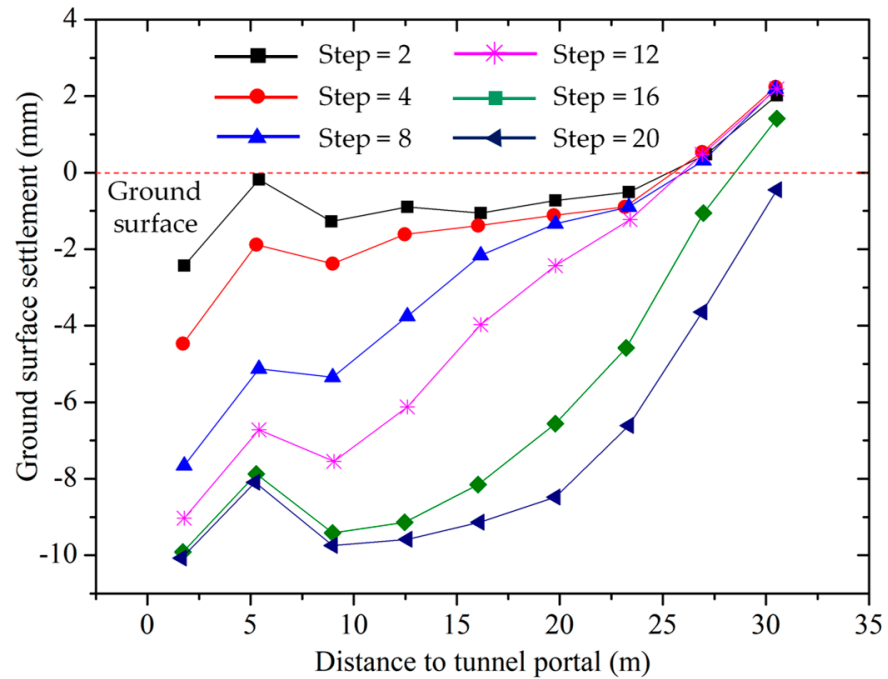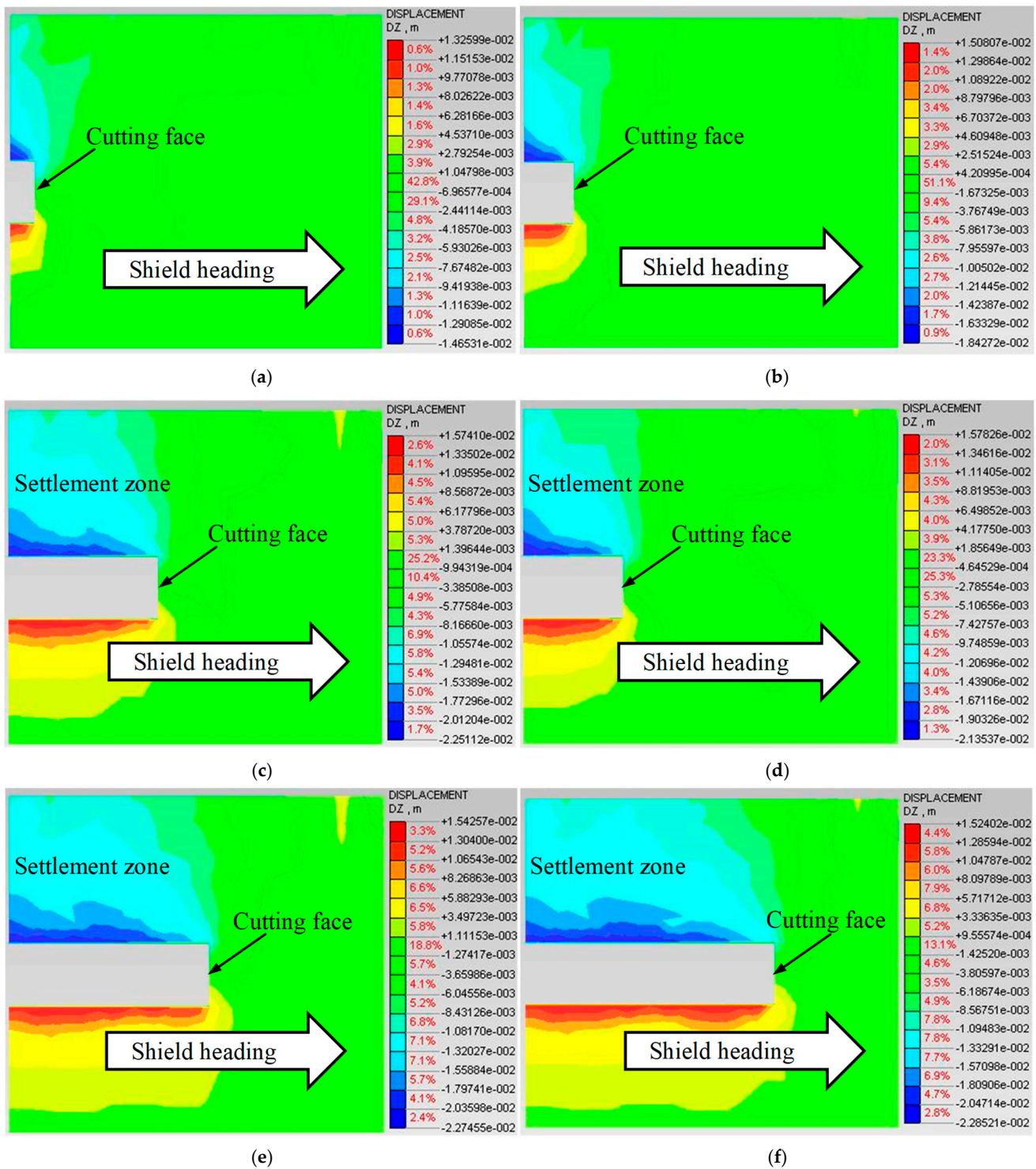
Figure 4. The surface settlement in the longitudinal direction at different excavation steps.

The excavation process involves the removal of soil at a length of 24 m per cycle. The vertical displacement of the soil around the tunnel is depicted in Figure 5. Notably, the soil displacement is significantly greater near the tunnel and varies along its length. The soil above the tunnel exhibits downward displacement, whereas the soil beneath it shows an upward trend. The maximum downward displacement recorded is 22.8 mm, and the maximum upward displacement is 15.7 mm. This displacement diminishes progressively with an increasing distance from the tunnel's radius. The tunnel face experiences greater displacement as excavation progresses, and the displacement of soil previously removed increases with each excavation step. Consequently, shield tunneling exerts a significant impact on soil displacement.

3.2. Surface Settlements with Different Overburden Depths

Figure 6 illustrates the surface settlement at section K18 + 288.163 for varying cover depths of 10 m, 14 m, 18 m, and 22 m. The settlement profiles across all sections exhibit a comparable pattern, with the maximum settlement consistently occurring above the tunnel's central axis. At point A (K18 + 288.163), the surface settlement values escalate to −14.34 mm, −14.89 mm, −15.17 mm, and −16.41 mm as the shield machine's cover depth increases from $Z = 0$ m (ground level) to $H = 10$ m, 14 m, 18 m, and 22 m (the overburden soil layer thickness), respectively. To verify the feasibility of the results of the study, the results are compared with those in the existing literature [50–56].

In this study, we compared the maximum ground surface settlements across four scenarios, each with soil cover layers with varying thicknesses, H, as depicted in Figure 7. The analysis reveals that the soil cover layer exerts a limited influence on the transverse settlement profile. Specifically, the maximum settlement reached 20.58 mm for $H = 10$ at a distance D of 10 m, exceeding that for $H = 22$ by 4.02 mm. It is clear that when the cover depth H decreases, the maximum ground surface settlement increases. The amount of settlement at the observation location decreases as the soil cover layer becomes thicker, yet this reduction remains modest, akin to its effect on the transverse behavior.

Figure 5. Surface settlement in longitudinal direction at different excavation steps. Steps equal to (**a**) 2; (**b**) 4; (**c**) 8; (**d**) 12; (**e**) 16; and (**f**) 20.

3.3. Surface Settlements with Outer Shields with Different Diameters

When the outer tunnel diameter is 10 m and the cover depth is 14 m, the surface settlement at section K18 + 288.163 increases to a significant value of −19.19 mm, as shown in Figure 8. The occurrence of "ground rebound" is not consistent but can manifest sporadically. Conversely, when the outer tunnel diameter is reduced to 4 m with the cover depth remaining at 14 m, the maximum surface settlement recorded is −7.59 mm, significantly lower than that observed with a 10 m diameter. Figure 9 delineates the

characteristics of maximum ground surface settlement at section K18 + 288.163 under varying cover depths with different outer tunnel diameters. It is clear that a significant increase in ground surface settling is correlated with an increase in the outer tunnel width.
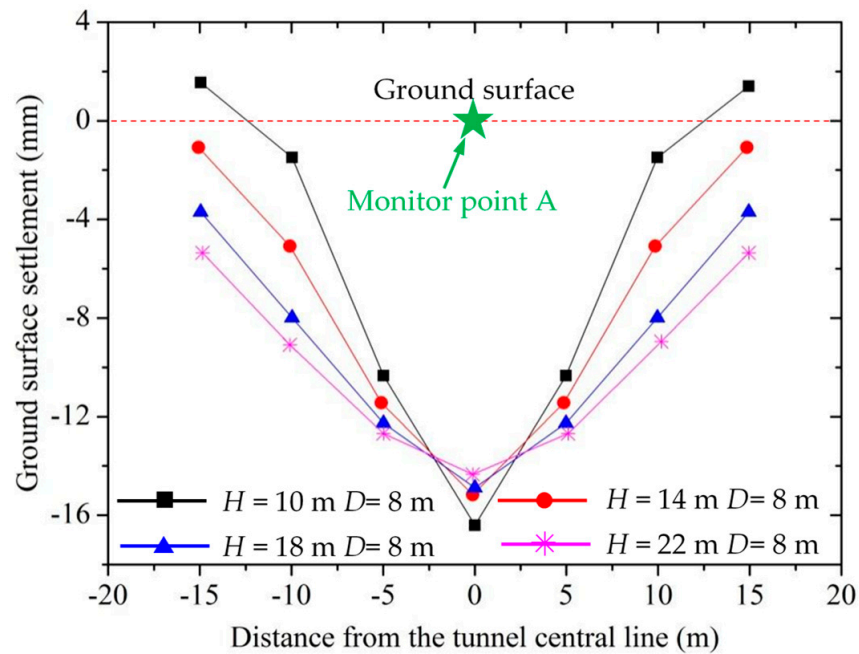

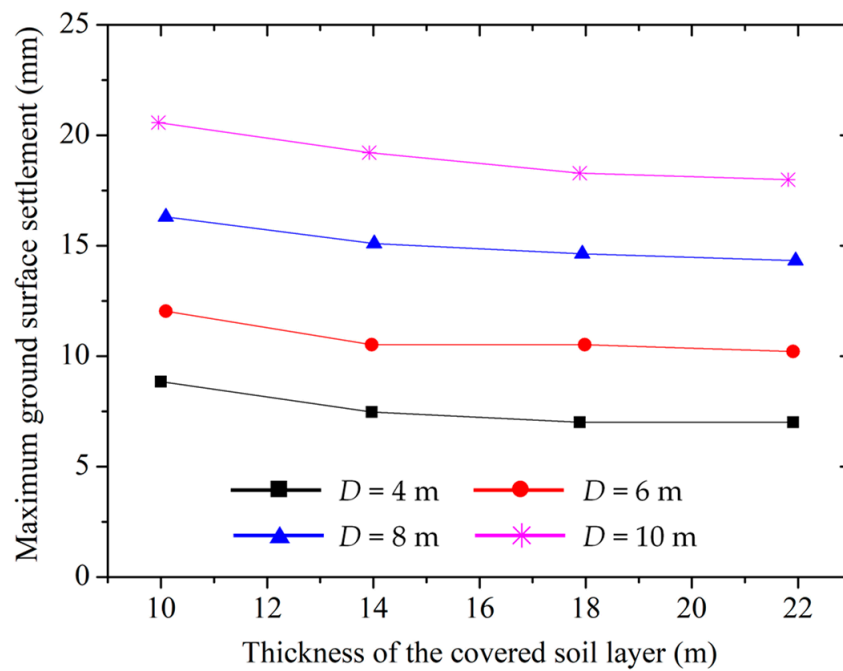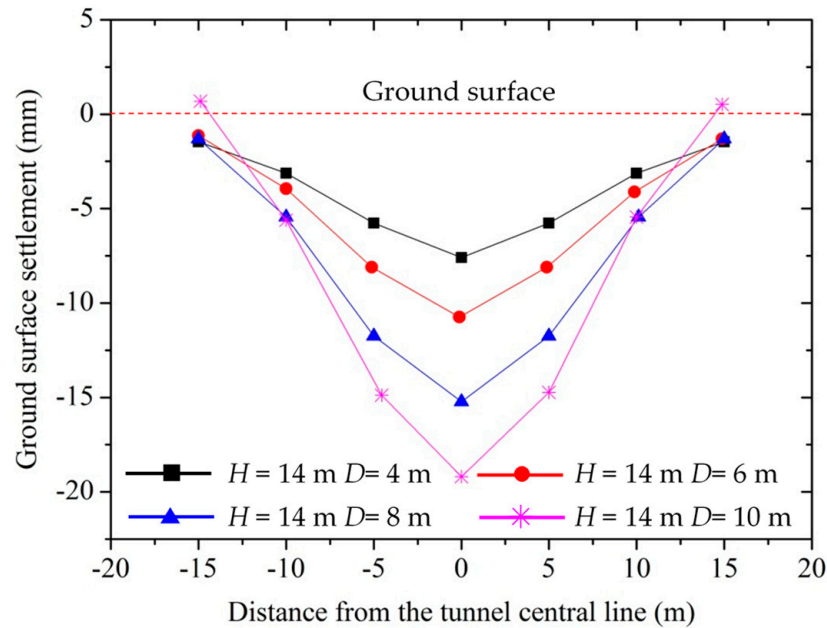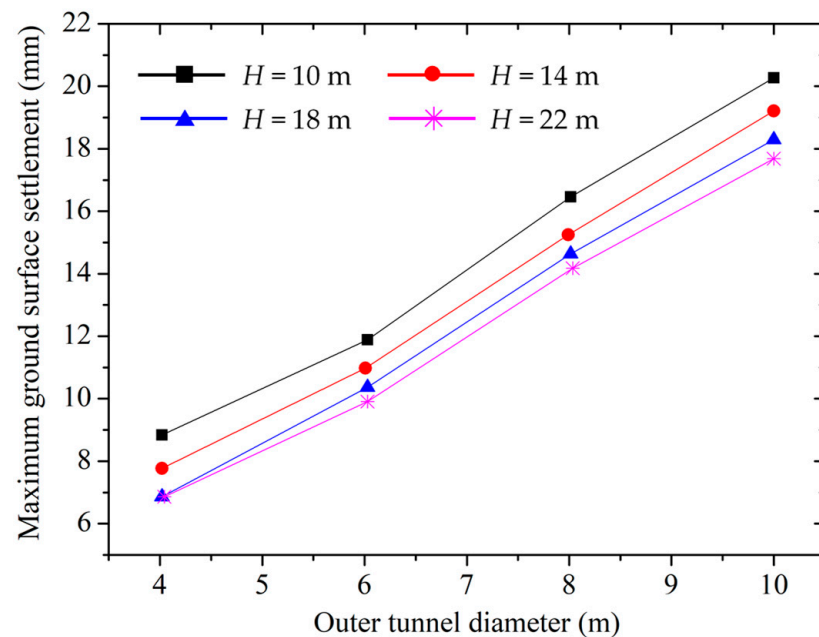**Figure 6.** Surface settlement trough at section K18 + 288.163 for different cover depths *H*.

Figure 7. The relationship between the maximum ground surface settlement and the thickness of the covered soil layer.

Figure 8. The surface settlement trough at section K18 + 288.163 for different outer tunnel diameters.

Figure 9. The relationship between the maximum ground surface settlement and the outer tunnel diameter.

3.4. The Surface Settlements with Different Grout Filling Rates of Shield Tail

The tunnel segments, each 1.2 m wide, are assembled under the protective shield shell, which imparts greater rigidity and minimizes ground settlement due to its structural integrity. As the shield advances, the tail segment becomes exposed, necessitating grouting to fill the void and mitigate further settlement. In order to evaluate their support independently of the shield shell, simulations of the segment and tail gap filling materials are carried out. Concurrently, pressure *P* is applied to the excavation face to emulate the earth pressure exerted by the shield, facilitating a simulation of the shield construction process.

The initial 3D equilibrium of the surrounding soil may be upset by inadequate or postponed grouting at the shield tail, which could cause soil displacement in the direction of the void, tunnel-induced displacement, and surface settling. Synchronous and secondary

grouting are common engineering practices aimed at reducing surface settlement associated with shield tail voids. While a small grouting volume can partially counteract soil settlement, an excessive volume may result in ground uplift. Figure 10 shows the results of the FEM simulations used to assess the link between grouting volume and surface settlement at different filling rates (ψ). The findings show a linear relationship between lower maximum surface settlement and higher grout filling rates.
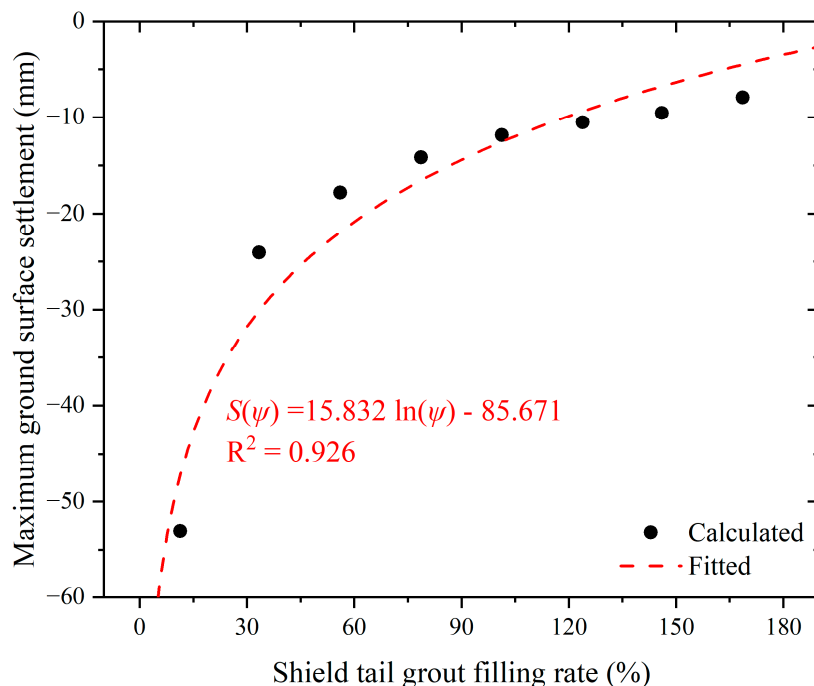

Figure 10. Relationship between maximum ground settlement and grout filling rate of shield tail.

Table 5 provides specifics on the soil layer as well as the mechanical and physical characteristics of the slurry and segments used in the K18 + 288.163 tunnel section computations.

Table 5. The mechanical parameters of the materials of the structural components.

Structural Element	Unit Weight (kN/m^3)	Modulus of Elasticity (MPa)	Poisson Ratio	Construction Technique
Duct piece	26	20.4×10^3	0.2	C50 reinforced concrete
Soft slurry	21	1.0	0.3	Cement slurry
Sclerosis slurry	21	50	0.25	Cement slurry

Synchronous or secondary grouting is extensively employed in engineering to mitigate ground settlement resulting from shield tail gaps. While a limited grouting volume can lead to partial ground subsidence, an excessive volume may induce ground heave. The specific filling rates, denoted by ψ, are calculated using the finite element method at 10%, 30%, 55%, 79%, 100%, 120%, 150%, and 170%. The summarized findings, as depicted in Figure 10, show that when the grouting filling rate increases, the maximum ground settlement decreases and may result in ground uplift. The relationship between these variables is fundamentally logarithmic, and the fitting relationship is as follows. The computational findings show that ground settlement is significantly impacted by the grouting rate at the shield tail, highlighting the importance of enhancing the filling rate at the shield tail as a key strategy to reduce ground subsidence.

$$S(\psi) = 15.832\mathrm{In}(\psi) - 85.671, \tag{6}$$

where ψ represents the grout filling rates; $S(\psi)$ represents the maximum ground surface settlement.

4. Discussion

4.1. Comparisons Between the Measured Surface Settlements and Different Calculation Methods

The numerical predictions were juxtaposed with field measurements at section K18 + 048.163, as depicted in Figure 11a. The highest surface settlement (S_{max}) of 7.82 mm, as determined using the numerical model, is only 27.1% (1.67 mm) greater than the measured value of 6.15 mm. Discrepancies are evident, with the actual ground movement at the observation point exhibiting a more intricate pattern than the simulations, characterized by occasional "up and down" fluctuations rather than a smooth, consistent trend. Furthermore, there is a 0 m deviation between the observed data's symmetry axis and the tunnel axis (origin in the diagram).
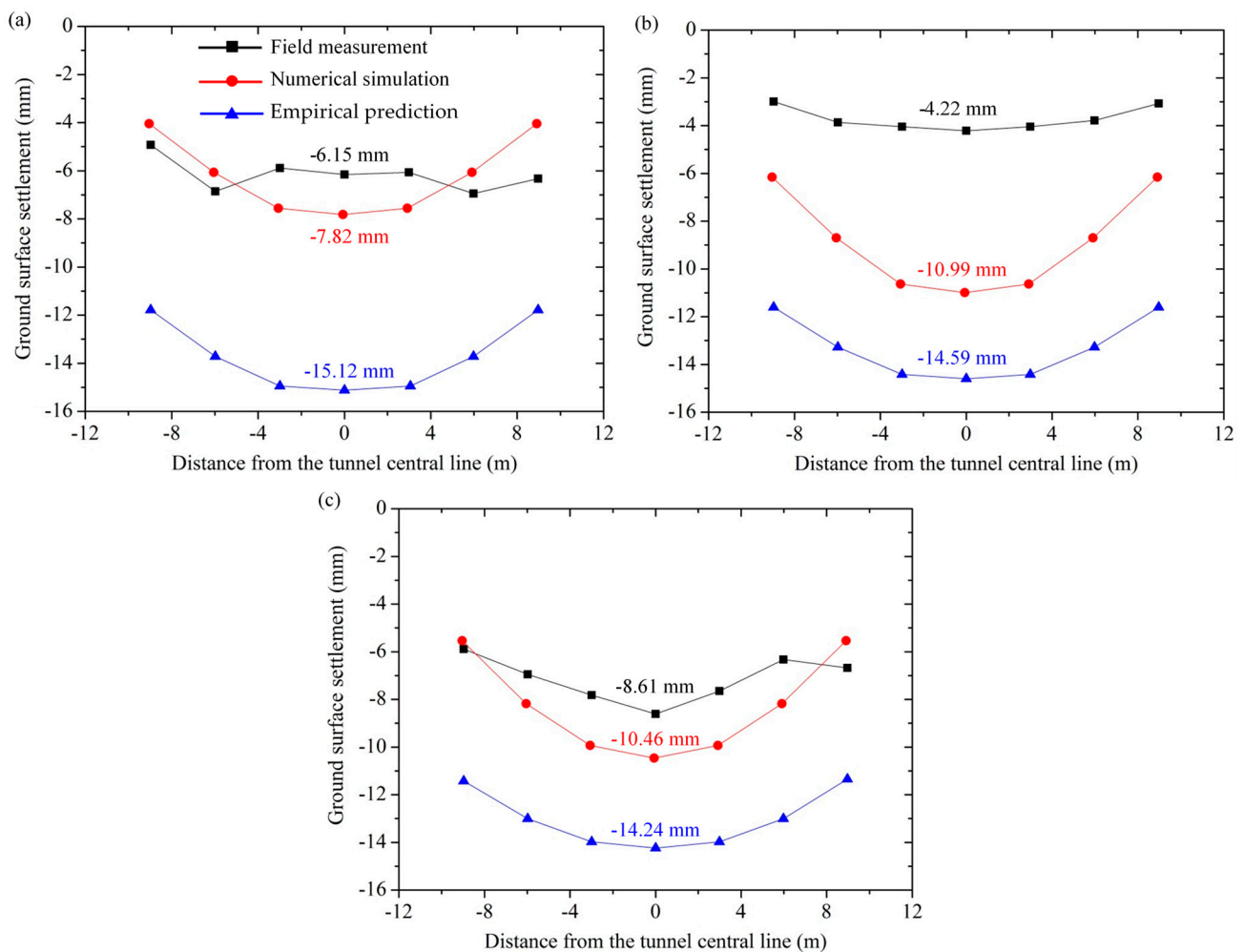
Figure 11. Comparison among measured, simulated, and computed surface settlement trough at (**a**) section K18 + 048.163, (**b**) section K18 + 192.163, and (**c**) section K18 + 288.163.

Figure 11b illustrates the transverse settlement curves at K18 + 192.163 during the shield machine's advancement to the 403rd ring. Despite minor anomalies in the measured curve, the three curves are broadly similar in shape and terminal values. For every curve shown in Figure 11b, the maximum surface settlement (S_{max}), trough width parameter (i), and volume loss (V_s) were determined using Equation (2).

In section K18 + 288.163, presented in Figure 11c, the maximum settlement reached 8.61 mm as the shield machine progressed to the 483rd ring. The measured settlement trough curve exhibits approximate symmetry with respect to the tunnel's central line. However, it displays fluctuations around the stability line, with occasional instances of "ground rebound." The left-hand measurement stations, which were over 10 m from the tunnel's center line, were notable for exhibiting a notable "heave" phenomenon.

4.2. The Influence Factors of Surface Settlement in Shield Tunneling

Several factors affect surface settlement when building shield tunnels, which this study examines individually using the Finite Element Method (FEM). Typically, surface settlement increases progressively with shield advancement (Figure 5); however, it decreases as one moves farther away from the tunnel's axis (Figure 3). For a constant excavation radius, a greater overburden thickness leads to a wider settlement trough and, consequently, a reduced maximum surface settlement (Figure 6). In essence, an increased overburden thickness extends the area affected by surface settlement. A linear correlation is observed between surface settlement increase and the shield's outer diameter, assuming a constant overburden thickness (Figures 7 and 8). Specifically, a larger excavation radius, for a given overburden thickness, results in greater soil loss per unit length and a more pronounced maximum ground settlement. The study's calculations indicate that the grout filling rate at the shield tail significantly impacts surface settlement, with an increased fill rate being crucial for mitigating settlement (Figure 11).

In addition to excavation circumstances, the mechanical and physical characteristics of the tunnel's foundation have a major impact on surface settlement brought on by tunneling. Figure 12 illustrates the surface settlement in the transverse direction for varying foundation deformation moduli, with all curves exhibiting a similar pattern. However, the maximum settlement values vary, with the highest being 2.75 times the lowest value, as depicted in Figure 12. This variation is attributed to the increased grouting volume resulting from the injection pipe.
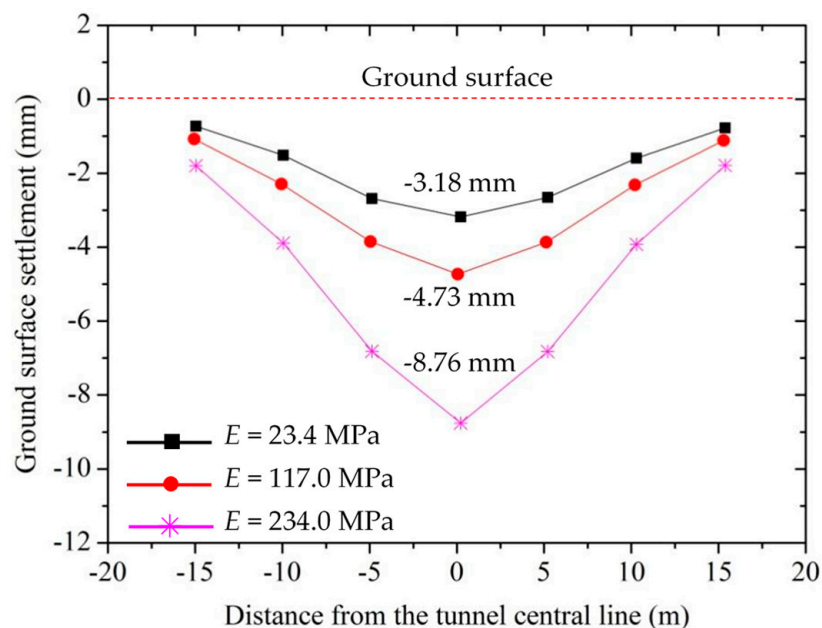

Figure 12. The surface settlement trough at section K18 + 288.163 for different elastic modulus values.

5. Conclusions

Using an upgraded FEM model in combination with the Midas GTS software, this study provides a thorough investigation of ground surface settlements related to the building of a large-diameter shield-driven tunnel for Shenyang Subway Line 2. The geological layers of Shenyang Subway Line 2 were incorporated into a computer model that was created to simulate the sequential construction of a 24 m tunnel through three separate segments. The model's simulated surface settlements correlated more closely with the actual measurements than those predicted using the Peck empirical formula. The findings reveal that maximum settlement typically occurs at approximately twice the equivalent diameter behind the excavation face. Surface settlement was inversely proportional to the overburden thickness (H), the soil's elastic modulus (E), and shield tail grout filling rate (ψ), and directly proportional to the shield's outer diameter (D). When H is equal to 10 m, 14 m, 18 m, and 22 m (section K18 + 288.163), the maximum settlement increases to -14.34 mm, -14.89 mm, -15.17 mm, and -16.41 mm. When E is equal to 23.4 MPa, 117.0 MPa, and 234.0 MPa (section K18 + 288.163), the maximum settlement increases to -3.18 mm, -4.73 mm, and -8.76 mm. This study suggests that increasing overburden soil thickness and reducing the excavation's outer diameter are effective strategies for mitigating surface settlement. In practice, surface settlement can be managed by soil reinforcement, and enhancing the shield tail filling rate is crucial for minimizing ground subsidence. For sections with stringent settlement requirements, slurry filling can be employed to reduce ground settlement. The developed model provides a valuable reference for understanding surface settlements along Shenyang Subway Line 2 and serves as a predictive tool for simulating and estimating surface settlements under various construction conditions in similar geotechnical engineering projects.

In numerical calculations, finer mesh sizes result in more complex computations, necessitating longer processing times and higher computer performance. Given the constraints of our computer's capabilities, the model presented here is of a smaller scale. It is anticipated that with advancements in computer performance, it will be possible to simulate a broader range of settlements, potentially covering the entire subway line. Accurately simulating the detailed excavation process of the shield, post-wall grouting, shoring, reinforcement, and interactions with adjacent structure foundations remain challenging. Therefore, future studies should aim to refine the model to address these limitations.

References

1. Xu, R.; Li, X.; Yang, W.; Rabiei, M.; Yan, C.; Xue, S. Field Measurement and Research on Environmental Vibration Due to Subway Systems: A Case Study in Eastern China. *Sustainability* **2019**, *11*, 6835. [CrossRef]
2. Feng, X.; Hou, D.; Huang, Z. The Influence of Shield Tunneling Characteristics on the Safety of Buildings Above-Case Study for Shanghai Zone. *Sustainability* **2022**, *14*, 13391. [CrossRef]
3. Gao, Y.; Liu, Y.; Tang, P.; Mi, C. Modification of Peck Formula to Predict Surface Settlement of Tunnel Construction in Water-Rich Sandy Cobble Strata and Its Program Implementation. *Sustainability* **2022**, *14*, 14545. [CrossRef]
4. Fang, Y.; Chen, Z.; Tao, L.; Cui, J.; Yan, Q. Model Tests on Longitudinal Surface Settlement Caused by Shield Tunnelling in Sandy Soil. *Sustain. Cities Soc.* **2019**, *47*, 101504. [CrossRef]
5. Wang, L.; Gong, G.; Shi, H.; Yang, H. Modeling and Analysis of Thrust Force for EPB Shield Tunneling Machine. *Autom. Constr.* **2012**, *27*, 138–146. [CrossRef]
6. Fang, Y.; He, C.; Nazem, A.; Yao, Z.; Grasmick, J. Surface Settlement Prediction for EPB Shield Tunneling in Sandy Ground. *KSCE J. Civ. Eng.* **2017**, *21*, 2908–2918. [CrossRef]
7. Xie, H.; Liu, Z.; Yang, H. Pressure Regulation for Earth Pressure Balance Control on Shield Tunneling Machine by Using Adaptive Robust Control. *Chin. J. Mech. Eng.* **2016**, *29*, 598–606. [CrossRef]
8. Bouayad, D.; Emeriault, F.; Maza, M. Assessment of Ground Surface Displacements Induced by an Earth Pressure Balance Shield Tunneling Using Partial Least Squares Regression. *Environ. Earth Sci.* **2015**, *73*, 7603–7616. [CrossRef]
9. Shao, C.; Lan, D. Optimal Control of an Earth Pressure Balance Shield with Tunnel Face Stability. *Autom. Constr.* **2014**, *46*, 22–29. [CrossRef]
10. Meng, Q.; Qu, F.; Li, S. Experimental Investigation on Viscoplastic Parameters of Conditioned Sands in Earth Pressure Balance Shield Tunneling. *J. Mech. Sci. Technol.* **2011**, *25*, 2259–2266. [CrossRef]
11. Cheng, H.; Chen, J.; Chen, G. Analysis of Ground Surface Settlement Induced by a Large EPB Shield Tunnelling: A Case Study in Beijing, China. *Environ. Earth Sci.* **2019**, *78*, 605. [CrossRef]
12. He, C.; Feng, K.; Fang, Y.; Jiang, Y. Surface Settlement Caused by Twin-Parallel Shield Tunnelling in Sandy Cobble Strata. *J. Zhejiang Univ. Sci. A* **2012**, *13*, 858–869. [CrossRef]
13. Xu, Q.; Zhu, H.; Ding, W.; Ge, X. Laboratory Model Tests and Field Investigations of EPB Shield Machine Tunnelling in Soft Ground in Shanghai. *Tunn. Undergr. Space Technol.* **2011**, *26*, 1–14. [CrossRef]
14. Fang, Y.; Yang, Z.; Cui, G.; He, C. Prediction of Surface Settlement Process Based on Model Shield Tunnel Driving Test. *Arab. J. Geosci.* **2015**, *8*, 7787–7796. [CrossRef]
15. Meguid, M.A.; Saada, O.; Nunes, M.A.; Mattar, J. Physical Modeling of Tunnels in Soft Ground: A Review. *Tunn. Undergr. Space Technol.* **2008**, *23*, 185–198. [CrossRef]
16. Nomoto, T.; Imamura, S.; Hagiwara, T.; Kusakabe, O.; Fujii, N. Shield Tunnel Construction in Centrifuge. *J. Geotech. Geoenvironmental Eng.* **1999**, *125*, 289–300. [CrossRef]
17. Sun, J.; Liu, J. Visualization of Tunnelling-Induced Ground Movement in Transparent Sand. *Tunn. Undergr. Space Technol.* **2014**, *40*, 236–240. [CrossRef]
18. Yuan, Y.; Jiang, X.; Liu, X. Predictive Maintenance of Shield Tunnels. *Tunn. Undergr. Space Technol.* **2013**, *38*, 69–86. [CrossRef]
19. Zhou, Z.; Ding, H.; Miao, L.; Gong, C. Predictive Model for the Surface Settlement Caused by the Excavation of Twin Tunnels. *Tunn. Undergr. Space Technol.* **2021**, *114*, 104014. [CrossRef]
20. Gui, M.-W.; Chen, S.-L. Estimation of Transverse Ground Surface Settlement Induced by DOT Shield Tunneling. *Tunn. Undergr. Space Technol.* **2013**, *33*, 119–130. [CrossRef]
21. Verruijt, A.; Booker, J.R. Surface Settlements Due to Deformation of a Tunnel in an Elastic Half Plane. *Geotechnique* **1998**, *48*, 709–713. [CrossRef]
22. Park, K.-H. Analytical Solution for Tunnelling-Induced Ground Movement in Clays. *Tunn. Undergr. Space Technol.* **2005**, *20*, 249–261. [CrossRef]
23. Zhu, C.; Li, N. Prediction and Analysis of Surface Settlement Due to Shield Tunneling for Xi'an Metro. *Can. Geotech. J.* **2017**, *54*, 529–546. [CrossRef]
24. Zhu, C. Control of Surface Settlement by Considering Shield Tunneling Technology. *KSCE J. Civ. Eng.* **2017**, *21*, 2896–2907. [CrossRef]
25. Beer, G.; Swoboda, G. On the Efficient Analysis of Shallow Tunnels. *Comput. Geotech.* **1985**, *1*, 15–31. [CrossRef]
26. Lee, K.M.; Rowe, R.K. An Analysis of Three-Dimensional Ground Movements: The Thunder Bay Tunnel. *Can. Geotech. J.* **1991**, *28*, 25–41. [CrossRef]
27. Sterpi, D.; Cividini, A. A Physical and Numerical Investigation on the Stability of Shallow Tunnels in Strain Softening Media. *Rock Mech. Rock Eng.* **2004**, *37*, 277. [CrossRef]
28. Brinkgreve, R.B.J. Selection of Soil Models and Parameters for Geotechnical Engineering Application. In *Soil Constitutive Models: Evaluation, Selection, and Calibration*; ASCE: Reston, VA, USA, 2005; pp. 69–98.

29. Gong, W.; Luo, Z.; Juang, C.H.; Huang, H.; Zhang, J.; Wang, L. Optimization of Site Exploration Program for Improved Prediction of Tunneling-Induced Ground Settlement in Clays. *Comput. Geotech.* **2014**, *56*, 69–79. [CrossRef]

30. You, X.; Liu, C.; Gong, Q.; Zhou, S. A Probabilistic Design Approach for Load of Metro Tunnel Induced by Surrounding Development: Part a: Determination of Development Intensity. *Tunn. Undergr. Space Technol.* **2018**, *79*, 52–66. [CrossRef]

31. Li, C.; Wang, Z.; Liu, Q. Numerical Simulation of Mudstone Shield Tunnel Excavation with ABAQUS Seepage–Stress Coupling: A Case Study. *Sustainability* **2023**, *15*, 667. [CrossRef]

32. Chen, S.-L.; Lee, S.-C.; Wei, Y.-S. Numerical Analysis of Ground Surface Settlement Induced by Double-o Tube Shield Tunneling. *J. Perform. Constr. Facil.* **2016**, *30*, 4016012. [CrossRef]

33. Chen, S.-L.; Gui, M.-W.; Yang, M.-C. Applicability of the Principle of Superposition in Estimating Ground Surface Settlement of Twin-and Quadruple-Tube Tunnels. *Tunn. Undergr. Space Technol.* **2012**, *28*, 135–149. [CrossRef]

34. Gao, L.X.; Yang, X.J.; Qin, L.K. Finite Element Analysis of the Surface Settlement Induced by the Shield Tunnel Construction. *Appl. Mech. Mater.* **2014**, *501*, 111–114. [CrossRef]

35. Mathew, G.V.; Lehane, B.M. Numerical Back-Analyses of Greenfield Settlement during Tunnel Boring. *Can. Geotech. J.* **2013**, *50*, 145–152. [CrossRef]

36. Oh, J.-Y.; Ziegler, M. Investigation on Influence of Tail Void Grouting on the Surface Settlements during Shield Tunneling Using a Stress-Pore Pressure Coupled Analysis. *KSCE J. Civ. Eng.* **2014**, *18*, 803–811. [CrossRef]

37. Kao, C.C.; Chen, C.-H.; Hwang, R.N. Mechanism of Ground Settlements and Heaves Due to Shield Tunneling. *J. Geoengin.* **2009**, *4*, 63–72.

38. Shi, X.; Cao, Y.; Rong, C.; An, G.; Wang, H.; Cui, L. Influence of Pipeline Leakage on the Ground Settlement around the Tunnel during Shield Tunneling. *Sustainability* **2022**, *14*, 16802. [CrossRef]

39. Jiang, Z.Y.; Yu, J. The Analysis of Stratum Settlement for a Large Diameter Slurry Shield Obliquely Under-Passing Embankment of the Yangtze River. *Adv. Mater. Res.* **2014**, *919*, 895–901. [CrossRef]

40. Wang, J.X.; Zou, B.P.; Chen, X.J.; Yi, J.; Kuang, G.L. Analysis of the Carbon Monoxide Released Law Caused by Shield Construction in Shallow Stratum in Sea Reclamation District. In *Proceedings of the New Frontiers in Engineering Geology and the Environment: Proceedings of the International Symposium on Coastal Engineering Geology, ISCEG-Shanghai 2012*; Springer: Berlin/Heidelberg, Germany, 2013; pp. 227–232.

41. Xie, X.; Yang, Y.; Ji, M. Analysis of Ground Surface Settlement Induced by the Construction of a Large-Diameter Shield-Driven Tunnel in Shanghai, China. *Tunn. Undergr. Space Technol.* **2016**, *51*, 120–132. [CrossRef]

42. Liang, J.; Tang, X.; Wang, T.; Lin, W.; Yan, J.; Fu, C. Analysis for Ground Deformation Induced by Undercrossed Shield Tunnels at a Small Proximity Based on Equivalent Layer Method. *Sustainability* **2022**, *14*, 9972. [CrossRef]

43. Peck, B.B. Deep Excavation and Tunnelling in Soft Ground, State of the Art Volume. In Proceedings of the 7th ICSMFE, Mexico City, Mexico, 25–29 August 1969; Volume 4, pp. 225–290.

44. Hosseini, S.A.A.; Mohammadnejad, M.; Hoseini, S.M.; Mikaeil, R.; Tolooiyan, A. Numerical and Analytical Investigation of Ground Surface Settlement Due to Subway Excavation. *Geosciences* **2012**, *2*, 185–191. [CrossRef]

45. Oteo, C.; Moya, J.F. Estimation of the Soil Parameters of Madrid in Relation to the Tunnel Construction. In Proceedings of the Seventh European Conference on Soil Mechanics and Foundation Engineering, Brighton, UK, 10–13 September 1979; Volume 3, pp. 239–247.

46. Migliazza, M.; Chiorboli, M.; Giani, G.P. Comparison of Analytical Method, 3D Finite Element Model with Experimental Subsidence Measurements Resulting from the Extension of the Milan Underground. *Comput. Geotech.* **2009**, *36*, 113–124. [CrossRef]

47. Romo, M.P.; Diaz, M. Face Stability and Ground Settlement in Shield Tunneling. In Proceedings of the Tenth International Conference on Soil Mechanics and Foundation Engineering, Stockholm, Sweden, 15–19 June 1981.

48. Knothe, S. Observations of Surface Movements under Influence of Mining and Their Theoretical Interpretation. In Proceedings of the European Congress on Ground Movement, Leeds, UK, 9–12 April 1957; pp. 9–12.

49. Caliri, M.F., Jr.; Ferreira, A.J.M.; Tita, V. A Review on Plate and Shell Theories for Laminated and Sandwich Structures Highlighting the Finite Element Method. *Compos. Struct.* **2016**, *156*, 63–77. [CrossRef]

50. Wang, F.; Du, X.L.; Li, P.F. Predictions of ground surface settlement for shield tunnels in sandy cobble stratum based on stochastic medium theory and empirical formulas. *Undergr. Space* **2023**, *11*, 189–203. [CrossRef]

51. Li, E.C.; Gao, Q.C.; Li, X.; Mao, T.Q.; Zheng, B. Displacement response characteristics of different sand tunnel excavation faces under true triaxial loading. *Front. Earth Sci.* **2023**, *10*, 1022719. [CrossRef]

52. Sohaei, H.; Hajihassani, M.; Namazi, E.; Marto, A. Experimental study of surface failure induced by tunnel construction in sand. *Eng. Fail. Anal.* **2020**, *118*, 104897. [CrossRef]

53. Andrea, F.; Alec, M.M.; Brinkgreve, R.B.J. Empirical and semi-analytical methods for evaluating tunnelling-induced ground movements in sands. *Tunn. Undergr. Space Technol.* **2019**, *88*, 47–62. [CrossRef]

54. Cao, L.Q.; Chen, X.S.; Lu, D.C.; Zhang, D.L.; Su, D. Theoretical prediction of ground settlements due to shield tunneling in multi-layered soils considering process parameters. *Undergr. Space* **2024**, *16*, 29–43. [CrossRef]

55. Zhang, F.; Huang, L.C.; Liang, Y. Calculation of Soil Deformation Caused by Shield Tunneling through the Sludge Layer with Plastic Drainage Plates. *Adv. Civ. Eng.* **2020**, 6625132. [CrossRef]

56. Wang, Y.; Dai, F.; Ding, B.S.; Zhong, M.; Zhang, H. Study on the efect of excavation sequence of three hole shield tunnel on surface settlement and segment deformation. *Sci. Rep.* **2023**, *13*, 16971. [CrossRef]